Journal of
Materials Chemistry B

Accepted Manuscript

This article can be cited before page numbers have been issued, to do this please use: L. Gui, J. zhou, L. Zhou and S. Wei, *J. Mater. Chem. B*, 2018, DOI: 10.1039/C8TB00334C.

ROYAL SOCIETY OF CHEMISTRY

rsc.li/materials-b

View Article Online
DOI: 10.1039/C8TB00334C

Journal Name

ARTICLE

A smart Copper-phthalocyanine framework nanoparticle for enhance hypoxic photodynamic therapy by weakening cell through ATP depletion

Received 00th January 20xx,
Accepted 00th January 20xx

DOI: 10.1039/x0xx00000x

www.rsc.org/

Li Gui, Jiahong Zhou, Lin Zhou*, Shaohua Wei*

Solid tumor hypoxia hinder photodynamic therapy (PDT) efficacy. Adenosine triphosphate (ATP) generation route of hypoxia tumor cells was an ineffective glycolysis processes, but ATP is crucial for rapid and uncontrolled growing and dividing. ATP depletion would inhibit DNA replication and glutathione (GSH) biosynthesis, which could inhibit its proliferation and make it sensitive to PDT treatment. In this regard, a nanoscale metal-organic framework nanoparticle, consisted of Cu^{2+} and carboxyl modified zinc phthalocyanine (ZnPc-$(COOH)_8$) ({Cu_8(ZnPc-$(COOH)_8$)}n, ZPCN), was design and prepared. In the dark cycle, ATP could deprive Cu^{2+} from ZPCN and form copper-ATP complex. ATP in above complex could be destroyed by copper mediated Fenton reaction and finally induce ATP depletion to inhibit its proliferation and make it sensitive to PDT treatment. In the light cycle, ZPCN could generate abundant cytotoxic reactive oxygen species to suppress tumor growth. These results demonstrated the potential applicability of the new strategy to overcome hypoxic tumor treatment by PDT.

Introduction

As a noninvasive treatment for cancer, PDT has received considerable attention in recent years. PDT employs light-excited photosensitizers (PS) to activate the transformation of surrounding O_2 into cytotoxic reactive oxygen species (ROS), such as singlet oxygen ($^1O_2$), H_2O_2, superoxide radical ($O_2^{\cdot -}$) and hydroxyl radical (·OH), to cause irreversible damage to malignant cells. [1, 2] Furthermore, under appropriate light irradiation position control at tumor site, PDT offers the advantage of an effective and selective method of destroying diseased tissues without damaging adjacent healthy ones for tumor targeting treatment. [3] Hypoxia, which is caused by an inadequate oxygen supply, is increasingly being recognized as a characteristic feature of solid tumors. [4-6] Hypoxia is believed to be one of the major causes for the failure of many kinds of cancer treatment, including chemotherapy (by up-regulating drug efflux P-glycoprotein expression to enhance drug resistance), [7, 8] radiotherapy (by decreasing ionizing radiation effect), [9] photothermal therapy (by up-regulating heat resistance heat shock proteins expression) [10, 11] and PDT. [12] PDT depends on the ability of light irradiated PS to transfer energy from light to the surrounding O_2 to generate cytotoxic ROS to kill tumor cells. [13, 14] In other words, the therapeutic outcome of PDT is strong O_2 dependent. [15 16] In light of this, integration of a PDT system with high activity under hypoxia condition could be promising for enhanced anticancer therapy.

To solve this problem, several different strategies were exploited to overcome tumor hypoxia and to improve the therapeutic effect. The first effective strategy is increasing O_2 concentration to relieve hypoxia by in situ catalase H_2O_2 to generate O_2 or directly delivering O_2 to hypoxic tumor. [4, 17-19] Another very useful strategy is combining PS with a hypoxia-activated prodrug to contribute a highly effective synergistic cancer therapy. [20, 21] Beyond that, using vascular-disrupting agents (VDA) to effectively starve the tumor to death, by depriving it of vital nutrients and oxygen, leading to tumor necrosis, is another good option to obtain satisfied treatment efficacy. [22]

ATP, a nucleoside triphosphate, is classified as the most important energy source for most of the physiological biochemical process. Hypoxic cancer cells ATP generation rely on glycolysis processes which is an ineffective ATP generation route comparing with well-oxygenated conditions. Cancer cells are strong ATP dependent to support their unique physiological processes, such as active DNA replication and high levels of GSH to build a strong antioxidant defence, to maintain their rapid and uncontrolled growing and dividing. [23-26] DNA replication is the cornerstone for cancer cell proliferation and GSH could consume ROS and sharply reduce PDT activity. Therefore, we proposed that if we deplete ATP in hypoxic cancer cells, they would weak and be more sensitive to PDT treatment to obtain the highly effective cancer therapy under hypoxic condition.

College of Chemistry and Materials Science, Jiangsu Key Laboratory of Biofunctional Materials, Jiangsu Collaborative Innovation Centre of Biomedical Functional Materials, Key Laboratory of Applied Photochemistry, Nanjing Normal University Nanjing (210023) P. R. China.
**E-mail: zhoulin@njnu.edu.cn (L. Zhou); shwei@njnu.edu.cn (S. H. Wei);*
Tel: +86-025-8589-1761

View Article Online
DOI: 10.1039/C8TB00334C

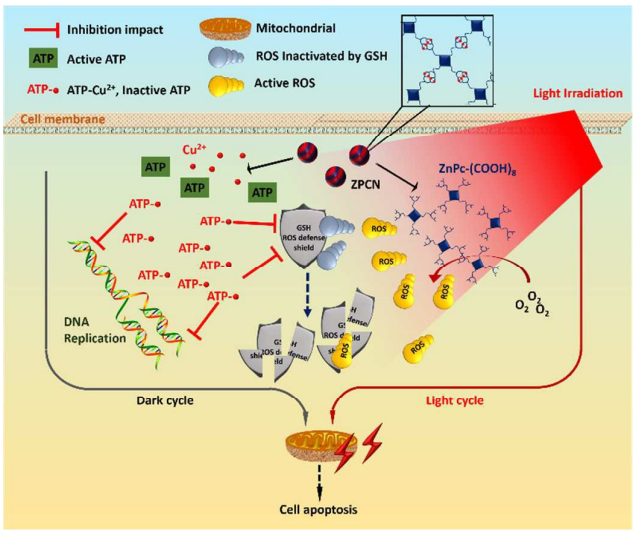

Scheme 1 Schematic presentation of anticancer mechanism of ZPCN.

To verify this hypothesis, herein, a new nanoscale metal-organic framework nanoparticle, consisted of Cu^{2+} and carboxyl modified ZnPc-$(COOH)_8$ based on the bond between Cu^{2+} and COO ($\{Cu_8(ZnPc\text{-}(COOH)_8)\}_n$, ZPCN), [27, 28] was prepared and used for hypoxic cancer treatment. As shown in scheme 1, ZPCN maintain inactive state during the delivery process in blood because during this process, it maintains in aggregation form. After been entrapped by cancer cells, ATP could deprive Cu^{2+} from ZPCN and make its disaggregation because of the higher affinity of phosphate to Cu^{2+} than that of COO [29] and the active ZnPc-$(COOH)_8$ was released. Similar like Fe^{3+}, Cu^{2+} is also an effective Fenton regent to generate hydroxyl radical. [30, 31] This fearsomely-reactive hydroxyl radical, once generated, attacks whatever it is next to. Its lifetime inside cell is vanishingly small, so, it reacts at its site of formation. [32] Therefore, during the dark cycle of the treatment, the Fenton-type reaction, in which copper ion in its complex with ATP reacts with H_2O_2 (cancer cells would produce excessive amounts of H_2O_2 and cause significant increase of H_2O_2 level in the tumor microenvironment) [13, 33, 34] to form $^{\cdot}OH$ to damage ATP (because they are close enough) and induce its depletion inside cells. [35] ATP depletion could inhibit DNA replication and decrease GSH level to provide a weak and sensitive cell state for PDT. [36, 37] During the light cycle of treatment, ROS could be generated after light irradiation. Finally, the synergistic of above cycles could cause mitochondrial membrane potential hyperpolarization or depolarization and induce effective cell apoptosis under hypoxic condition. Therefore, the potential applicability of a new strategy to overcome hypoxic tumor treatment by PDT is successfully demonstrated.

Experimental

Chemicals

The 1, 8-diazabicyclo [5, 4, 0]-undec-7-ene (DBU), 4-Nitrophthalonitrile, dimethyl 5-hydroxyisophthalate, 9, 10-anthracenedip-ropionic acid (ADPA) and ATP was obtained from Sigma-Aldrich. Dulbecco's minimum essential medium (DMEM) was from Gibco. Fetal bovine serum (FBS) was from Sijiqing. ATP Assay Kit, 3-[4,5-dimethylthiazol-2-yl]-2,5-diphenyl tetrazoliumbromide (MTT), Hematoxylin and Eosin Staining Kit(H&E), 2,7-dichlorodi-hydrofluorescein diacetate (DCFH-DA), Dihydroethidium (DHE), Rhodamine 123, Cell Cycle Analysis Kit, Annexin V-FITC Apoptosis Detection Kit, GSH and GSSG Assay Kit were obtained from Beyotime. Mitotracker green, Lysotracker blue and singlet oxygen sensor green (SOSG) were from thermo fisher. BES-H_2O_2-Ac was from Wako Chemicals. The necessary solvents were used after purification according to the reported literature. Chromatographic purifications were performed on silica gel columns (300-400 mesh, Qingdao Haiyang Chemical Co., Ltd, China). All chemical reagents were obtained from commercial suppliers and used as received unless otherwise stated.

Characterization

Ultraviolet-Visible (UV-Vis) absorption spectra were obtained by a Varian Cary 50 spectrophotometer. Fluorescence spectra were recorded on a Cary Eclipse fluorometer. Infrared spectra were obtained by Bruker Tensor infrared spectrometer. Zeta potential was detected with Malvern Zetasizer Nano 90 measurements in aqueous system. Transmission Electron Microscope (TEM) images were got by Hitachi H7650 transmission electron microscope. Morphology and fluorescence inside cells was monitored by a Nikon Ti microscope and Nikon Ti-E-A1R confocal laser scanning microscope. ^{1}H NMR and ^{13}C NMR spectra were recorded using a Bruker Advance 400 MHz NMR spectrometer. Mass spectra were obtained on UltrafleXreme MALDI-TOF-MS spectrometer. Elemental analysis was measured by Vario MICRO Elementar. Fluorescence lifetime and fluorescence quantum yield were obtained using a Horiba Jobin Yvon FM-4P-TCSPC system. Flow Cytometry (FCM) analysis was carried on a Beckman XL flow cytometer. Differential thermal analysis (TG-DTA) was taken on Perkin Elmer Diamond TG-DTA analyser in N_2 atmosphere at a heating rate of 10 °C min^{-1}. A 665 nm LED (5 W) was used as light source.

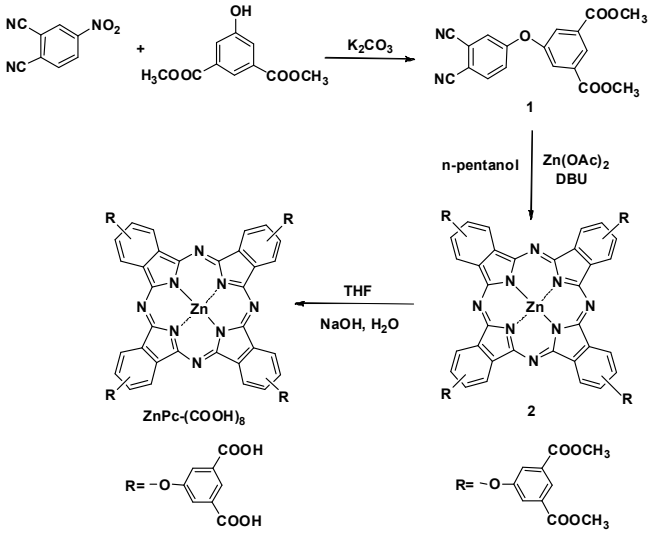

Scheme 2 The synthetic route of ZnPc-$(COOH)_8$.

View Article Online
DOI: 10.1039/C8TB00334C

Synthesis of ZnPc-(COOH)$_8$

ZnPc-(COOH)$_8$ was synthesized using our previous methods. [38] All the compounds were detected by melting point (M.P.), infrared spectra (IR), ^{1}H Nuclear Magnetic Resonance Spectra (^{1}H NMR) and UltraflexXreme MALDI-TOF-MS. ZnPc-(COOH)$_8$ synthetic route was shown in Scheme 2.

Compound **1** was synthesized as following process. Under N_2 atmosphere, 4-nitrophthalonitrile (0.25 g, 1.45 mmol), dimethyl 5-hydroxyisophthalate (0.30 g, 1.45 mmol) and potassium carbonate (0.29 g, 2.89 mmol) were mixed in 8 mL DMF was stirred at 75 °C for 8 h. Then, 50 mL water was added into the solution after it cooling to room temperature and the product was extracted by ethyl acetate. The impurities in ethyl acetate were removed by washing ethyl acetate solution using water and saturated sodium chloride for 3 times. Ethyl acetate was removed by vacuum distillation. The obtained product was further purified by silica gel column chromatography using ethyl acetate / petroleum ether (1:2, v/v). Finally, pure compound **1** as white solid was obtained (454.9 mg, 92.6%). M.P. was 125 °C; IR (KBr, ν_{max}/cm^{-1}): 3425, 3084, 2233, 1735, 1584, 1493, 1316, 1264, 1008, 837, 765. ^{1}H-NMR (400 MHz, DMSO-d_6): δ/ppm: 8.32 (t, 1H, J=1.6 Hz, Ar), 8.13 (d, 1H, J=8.8 Hz, Ar), 7.90 (d, 2H, J=1.6 Hz, Ar), 7.86 (d, 1H, J=2.8 Hz, Ar), 7.54 -7.51 (m, 1H, Ar). ^{13}C-NMR (100 MHz, DMSO-d_6): δ /ppm: 165, 160.7, 154.9, 136.8, 133.0, 126.9, 125.7, 123.6, 123.3, 117.3, 116.2, 115.7, 109.7. Anal. Calcd for $C_{18}H_{12}N_2O_5$: C, 64.29; H, 3.60; N, 8.33. Found: C, 64.31; H, 3.57; N, 8.29.

ZnPc-(COOH)$_8$ was synthesized by following protocols. Under N_2 atmosphere, compound **1** (0.25 g, 0.75 mmol) and $Zn(OAc)_2$ (0.09 g, 0.47 mmol) were added to 8 mL dried n-pentanol and stirred at 90 °C for 1 h. Then, DBU (0.1 mL, 0.67 mmol) was added and the mixture was heated to 130 °C and stirred for another 12 h. Then, the solvents were removed under reduced pressure. Silica gel column chromatography using ethyl acetate / petroleum ether (1:2, v/v) and methanol/ dichloromethane (1:5, v/v) was used to purify the product. The vacuum-dried product was washed by NaOH and methanol (1:4, v/v, 50 mL) at 60 °C for 12 h. The impurities were removed by filtration. Then, 10% HCl was added to above solution drop by drop until many dark green solid precipitates. Above purification process was repeated 3 times to obtain pure ZnPc-(COOH)$_8$ (0.06 g, 24.3%). M.P.>200 °C, IR (KBr, ν_{max}/cm^{-1}): 3436, 3083, 2922, 1710, 1593, 1463, 1265, 1227, 1116, 974, 838, 758.^{1}H-NMR (400 MHz, DMSO-d_6): δ/ppm: 13.37 (br, 8H, COOH), 8.93-8.54 (m, 4H, Pc-H), 8.34-7.76 (m, 12H, Ar), 7.47-7.24(m, 8H, Pc-H). HRMS (MALDI-TOF) m/z: 1296.682, (Calculated. For $C_{64}H_{32}N_8O_{20}Zn$: 1296.102). Anal. Calcd for $C_{64}H_{32}N_8O_{20}Zn$: C, 59.20; H, 2.48; N, 8.63. Found: C, 59.19; H, 2.47; N, 8.65.

{Cu$_8$(ZnPc-(COOH)$_8$)}$_n$ (ZPCN) preparation

100 μL of ZnPc-(COOH)$_8$ (10 mM) and 100 μL of $CuCl_2$ solution (160 mM) were mixed in 10 mL Tris-HCl buffer (pH =7.4). The mixture was stirred for 30 min to form ZPCN. The result ZPCN was purified by dialysis the solution using a 12-14 kDa cut-off cellulose membrane for 24 h to water.

Chemical method to detect $^1O_2$

$^1O_2$ was detected using ADPA because it could interact with $^1O_2$ to generate its endoperoxide, which induce its absorbance intensity decreasing. The mixture of 3 mL drugs solutions and 150 μL ADPA (5.5 mM) was irradiated by 665 nm light and their UV-Vis spectra changing were recorded. The decay of [ADPA] follows first order kinetics as the following Eq.

$$\ln([\mathbf{ADPA}]_t/[\mathbf{ADPA}]_0) = -kt$$

Where $[ADPA]_t$ and $[ADPA]_0$ are the concentrations of ADPA after and before irradiation, respectively. Therefore, the relative rate constant *k* can be extrapolated by a linear fit using the experimental points and calculated.

Cell culture

Human lung alveolar basal carcinoma epithelial cells (A549 cells) were cultured in DMEM containing FBS (10%, v/v), penicillin (100 U/mL) and streptomycin (100 μg/mL) in an incubator (Thermo Scientific) at 37 °C under an atmosphere of 5% CO_2 and 5% O_2 to simulate hypoxia microenvironment of solid tumour. [39]

Cellular intracellular distribution

A549 cells were seeded onto glass-bottom dishes at a density of 1×10^5 cells per dish in 1 mL of medium and incubated for 24 h before treatment of ZPCN, and ZnPc-(COOH)$_8$ separately. After 4 h incubation, DMEM with LysoTracker blue (100 nM) and Mitotracker green (100 nM) were replaced and incubated for 30 min before observation. LysoTracker was observed using a 405 nm laser; the emission wavelength was 425 to 475 nm and appeared blue. Mitotracker was observed using a 488 nm laser; the emission wavelength was 510 to 540 nm and appeared green. ZnPc-(COOH)$_8$ and ZPCN were observed using a 647 nm laser; the emission wavelength was 700 nm and appeared red.

Apoptosis assay by MTT and flow cytometry

The apoptosis of A549 cells induced by ZPCN, ZnPc-(COOH)$_8$ or free Cu^{2+} was studied by MTT and flow cytometry assay. Untreated A549 cells served as the control. To detect the dark toxicity, after exposure to various drug formulations, Cu^{2+}, ZPCN, and ZnPc-(COOH)$_8$, at equivalent concentrations (ZnPc-(COOH)$_8$: 7.5 μM; Cu^{2+}: 60 μM) for 48 hours in DMEM (10% FBS), MTT solution was added to each well to detect cell viability based on the absorption of the formazan product dissolved in DMSO. To detect the light induced toxicity, after exposure to various drug formulations, Cu^{2+}, ZPCN, and ZnPc-(COOH)$_8$, at equivalent concentrations (ZnPc-(COOH)$_8$: 7.5 μM; Cu^{2+}: 60 μM) for 24 hours, the cells were irradiated by light for 5 min. Then, the cells were re-incubated in incubator for 24 h and cell viability was detected using MTT assay. In addition, after re-incubation, cells were thoroughly washed with cold PBS and collected for treatment using Annexin V-FITC Apoptosis Detection Kit according to the manufacturer's protocol to detected cell apoptosis.

In vitro ATP deprivation detection

View Article Online
DOI: 10.1039/C8TB00334C

For determination of intracellular ATP concentration, A549 cells were seeded in 6-well plates at a density of 1×10^7 /well. After incubated in incubator for 12 h, the cells were treated by various drug formulations, Cu^{2+}, ZPCN, and ZnPc-$(COOH)_8$, at equivalent concentrations (ZnPc-$(COOH)_8$: 7.5 μM; Cu^{2+}: 60 μM) for 48 hours in DMEM (10% FBS) incubated overnight. After that, cells were washed with cold PBS and lysed with ATP lysis buffer. The ATP levels were measured according to the protocol of the ATP assay kit.

In vitro GSH deprivation detection

For determination of intracellular GSH concentration, A549 cells were seeded in 6-well plates at a density of 1×10^7 /well. After incubated in incubator for 12 h, the cells were treated by various drug formulations, Cu^{2+}, ZPCN, and ZnPc-$(COOH)_8$, at equivalent concentrations (ZnPc-$(COOH)_8$: 7.5 μM; Cu^{2+}: 60 μM) for 48 hours in DMEM (10% FBS) incubated overnight. After that, cells were washed with cold PBS and their GSH concentrations were measured according to the protocol of the GSH and GSSG Assay Kit.

In vitro ROS generation detection

Intracellular ROS generation was detected using following method. A549 cells were cultured in DMEM with 10% FBS with the density of 1×10^6 cells/mL in incubator for 24 h. Then, DMEM (10% FBS) with various drug formulations, Cu^{2+}, ZPCN, and ZnPc-$(COOH)_8$, at equivalent concentrations (ZnPc-$(COOH)_8$: 7.5 μM; Cu^{2+}: 60 μM) was replaced, separately. After 24 h incubation, DMEM with DCFH-DA (10 μM), DHE (5 μM), SOSG (10 μM) and BES-H_2O_2-Ac (5 μM) were replaced and incubated respectively for 30 min. Then, cells were washed with PBS for three times and irradiated for 5 min. Finally, cells were monitored by fluorescence microscopy.

Cell cycle analysis by flow cytometry

Flow cytometric analysis was performed to study the effect of various formulations of drug on the cell cycle. A549 cells were seeded in 24-well plates at a density of 1×10^7 /well. After incubated in incubator for 12 h, after exposure to various drug formulations DMEM solution (10% FBS), Cu^{2+}, ZPCN, and ZnPc-$(COOH)_8$, at equivalent concentrations (ZnPc-$(COOH)_8$: 7.5 μM; Cu^{2+}: 60 μM) for 24 hours, the cells were irradiated by light for 5 min. Then, the cells were re-incubated in incubator for 24 h. After that, cells were washed with PBS and their cell cycle were detected using cell cycle analysis Kit.

Mitochondria dysfunction detection

Methods for quantifying mitochondrial transmembrane potential based on rhodamine 123 fluorescence were similar to those reported previously. [40] Briefly, following experimental treatment, cultures were incubated for 30 min in DMEM containing 5 μM rhodamine 123. Cultures were washed with PBS and fluorescence was quantified using a flow cytometer (488 nm excitation).

In vivo biocompatibility and anti-tumour growth efficiency

Female BALB/c nude mice (3-4 weeks old) were purchased from Comparative Medicine Centre of Yangzhou University. All animal experiments were carried out in accordance with regulations of the Nanjing Committee of Use and Care of Laboratory Animals, and all experimental protocols were approved by the Animal Ethics Committee of Nanjing Normal University. For biocompatibility study, female Kunming mice were divided into 3 groups and intravenously injected through tail vein for saline, ZnPc-$(COOH)_8$ and ZPCN (ZnPc-$(COOH)_8$ per administration was 20 mg/kg, Cu^{2+} per administration was 160 mg/kg). Their body weight was recorded every day and after 20 days, the mice were sacrificed and their organs (heart, liver, spleen, lung, kidney, and brain) were taken out for the assessment using H&E staining for histological analysis.

For anti-tumor growth study, female BALB/c nude mice were subcutaneously injected with A549 cells to establish the tumor xenograft (tumor volume about 100 mm^3). The mice were divided into 3 groups including control group, ZnPc-$(COOH)_8$ and ZPCN (ZnPc-$(COOH)_8$ per administration was 1.5 mg/kg, Cu^{2+} per administration was 12 mg/kg). The drugs were intravenously injected through tail vein to nude mice 1 time every two days. 665 nm LED was used to irradiate the tumor position carried out after injection of drugs for 12 h. The body weight and the tumor volume were recorded every day. After 20 days, the mice were sacrificed and their tumor tissue were taken out for the assessment using H&E staining for histological analysis.

Statistical analysis

All biochemical experiments were performed in duplicate and an average of the results were used. Statistical analysis was done and the mean, standard deviation, standard error, and the significant changes were expressed as the mean ± SD. $P < 0.05$ was considered to be statistically significant.

Results and discussion

ZPCN formation and ATP triggered decomposition

The carboxylate group has strong affinity with Cu^{2+}. Therefore, we proposed that in ZPCN, each ZnPc-$(COOH)_8$ linker is coordinated to eight different $Cu_2(COO)_4$ paddlewheel units through the carboxylate groups and interconnects these binuclear paddlewheel units into 2D infinite layers. [27] All the parallel layers are slipped with each other and further stacked into a 3D supramolecular architecture through π-π stacking interactions. [41] To verify this hypothesis, the complexation processes between ZnPc-$(COOH)_8$ and Cu^{2+} was monitored clearly by UV-visible and fluorescence spectra by molar ratio methods. For the molar ratio method, a series of solutions containing different concentrations of Cu^{2+} and a constant concentration of ZnPc-$(COOH)_8$ (10 μM) were prepared, and the absorbance at a wavelength at 680 nm was plotted against the molar ratio of [Cu^{2+}] / [ZnPc-$(COOH)_8$]. Two straight lines of different slopes can be derived from the plot, and the molar ratio where the two lines cross reflects the composition of the complex. [42] And the results indicated that Cu^{2+} form 8:1 complexes with ZnPc-$(COOH)_8$ (Fig. 1). Besides, the two absorbance peaks of ZnPc-$(COOH)_8$ at 640 nm and 680 nm were ascribed to its aggregate and monomer form, separately.

View Article Online
DOI: 10.1039/C8TB00334C

Interaction between Cu^{2+} and ZnPc-$(COOH)_8$ induced ZnPc-$(COOH)_8$ aggregation. The PDT activity of aggregate was much lower than the monomer form. Therefore, ZPCN could

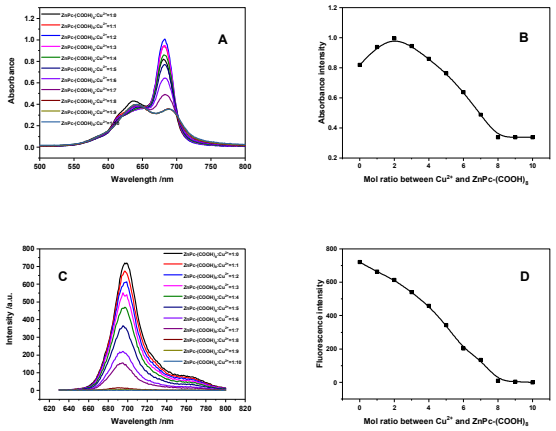

Fig. 1 (A) UV-Vis spectrum changes of ZnPc-$(COOH)_8$ in aqueous solution upon addition of Cu^{2+}. [ZnPc-$(COOH)_8$] = 10 μM, [Cu^{2+}] = 0, 10, 20, 30, 40, 50, 60, 70, 80, 90 and 100 μM; (B) Molar ratio plots for Cu^{2+}-ZnPc-$(COOH)_8$ obtained by plotting the absorbance at 680 nm as a function of the molar ratio of Cu^{2+} to ZnPc, (C) Fluorescence spectrum changes of ZnPc-$(COOH)_8$ in aqueous solution upon addition of Cu^{2+}. [ZnPc-$(COOH)_8$] = 10 μM, [Cu^{2+}] = 0, 10, 20, 30, 40, 50, 60, 70, 80, 90 and 100 μM; (D) Molar ratio plots for Cu^{2+}-ZnPc-$(COOH)_8$ obtained by plotting the fluorescence intensity at 695 nm as a function of the molar ratio of Cu^{2+} to ZnPc-$(COOH)_8$.

significantly minimized the ROS production efficiency of ZnPc-$(COOH)_8$. Similar results were detected in fluorescence results. The fluorescence of ZnPc-$(COOH)_8$ was sharply decreased after interacting with Cu^{2+} and also proved Cu^{2+} form 8:1 complexes with ZnPc-$(COOH)_8$. The formation of ZPCN was also proved by IR and TGA spectra (Fig. S2). As showing in Fig. 2, the 3D supramolecular ZPCN were well dispersed in aqueous solution with the average diameter of 50 nm.

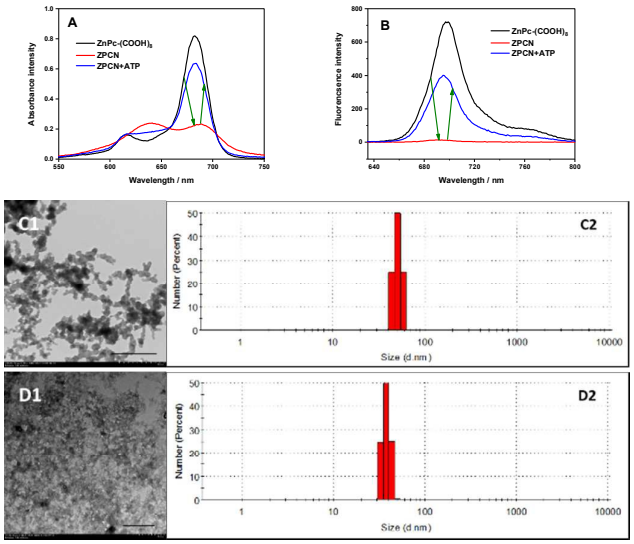

Fig. 2 (A) Absorbance spectra of ZnPc-$(COOH)_8$, ZPCN and ZPCN+ATP; (B) fluorescence emission spectra of ZnPc-$(COOH)_8$, ZPCN and ZPCN+ATP; (C) TEM image (1) and size distribution (2) of ZPCN; (D) TEM image (1) and size distribution (2) of ZPCN+ATP. Bar=200 nm.

Upon the introduction of ATP, the strong affinity between Cu^{2+} and ATP can promote the disassembly of the ZPCN and the process can be observed by monitoring the monomer form and fluorescence recovery of ZnPc-$(COOH)_8$. The disassemblyprocess was also verified by fluorescence life time and quantum yield regain results (Table S1). And TEM image also indicated that after ATP adding for 30 min, the structure of ZPCN was damaged and their size was decreased accordingly (Fig. 2).

$^1O_2$ generation ability and photobleaching property

As we mentioned above, forming ZPCN greatly induce ZnPc-$(COOH)_8$ aggregation, which could obviously minimize its $^1O_2$ generation capability. ATP adding could induce monomer recovering, which could cause $^1O_2$ generation capability recovering. To verify this hypothesis. $^1O_2$ generation ability of ZnPc-$(COOH)_8$, ZPCN and ZPCN+ATP were studied and compared. ADPA can react with $^1O_2$ to produce its endoperoxide, which would cause its absorption intensity decreasing. Fig. 3 shows the decrease in absorption intensity in different samples, including ZnPc-$(COOH)_8$, ZPCN and ZPCN+ATP, as a function of the time of light exposure. The absorption intensity of ZnPc-$(COOH)_8$ and ZPCN+ATP show a sharp decrease with the time of light exposure, indicating the generation of $^1O_2$. On the contrary, ZPCN produced almost no change in the absorption intensity of ADPA with the same irradiation time. The relative rate constant *k* of ZnPc-$(COOH)_8$, ZPCN and ZPCN+ATP were -1.26×10^{-2}, -0.03×10^{-2} and -0.93×10^{-2}. The $^1O_2$ generation ability of ZPCN and ZPCN+ATP were much higher than that of commercial photosensitizer porphyrin (k=-0.04×10^{-2}) under the same experiment condition. Above results confirmed that forming ZPCN could significantly minimized the $^1O_2$ production efficiency of ZnPc-$(COOH)_8$ and ATP could deprive Cu^{2+} in ZPCN and induce its $^1O_2$ production efficiency recovering.

All the Ps used in PDT are known to be degraded or when exposed to light. Such photobleaching of Ps can be either a disadvantage or an advantage. If the sensitizer bleaches too rapidly during illumination, tumor destruction may be incomplete. On the other hand, the photobleaching could be used to decrease the concentration of sensitizer in the body and thus shorten the period of photosensitivity in patients following PDT. [43] Thus, ideal PS should have efficient ROS generation capability to ensure its PDT efficacy and high photobleaching rates to avoid side effect after PDT treatment. Above results indicated that our PS have satisfied $^1O_2$ generation ability. Therefore, their photobleaching during $^1O_2$ generation process were detected and compared. As shown in Fig. 3, upon exposure to the 665 nm light, the color of ZnPc-$(COOH)_8$ (or ZPCN+ATP) in aqueous solution changed from blue to colorless and a distinct decrease in absorbance was observed, indicating their photobleaching process during $^1O_2$ generation process. On the contrary, no photobleaching was detected in ZPCN because ZnPc-$(COOH)_8$ existing in aggregate

View Article Online
DOI: 10.1039/C8TB00334C

form, which has low $^1O_2$ generation ability but strong photostability. These results indicated that ZPCN has efficient

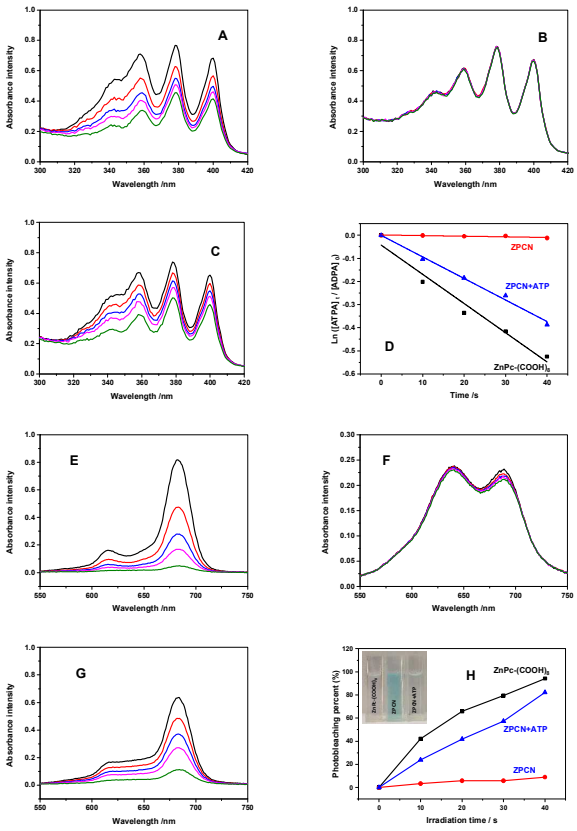

Fig. 3 Absorbance spectra of the drugs, including ZnPc-$(COOH)_8$ (A), ZPCN (B) and (C) ZPCN+ATP, with ADPA, after irradiation at 665 nm for 0, 20, 30 and 40 s. (D) The best fit to the experimental points of the same sample, where the value of k obtained; the absorption spectra of ZnPc-$(COOH)_8$ (E), ZPCN (F) and (G) ZPCN+ATP after irradiating with 665 nm LED; (H) photobleaching percent of ZnPc-$(COOH)_8$, ZPCN and ZPCN+ATP in 40 s irradiation; insert panel: colour of all drugs after irradiation for 40 s.

$^1O_2$ generation capability to ensure its PDT efficacy and high photobleaching rates to avoid side effect after PDT treatment.

Comparative Intracellular Localization.

The subcellular localization of PSs could also determine the outcome of PDT. [44] Although lysosomes were considered to be mere "waste bags" used by the cell to dispose of unwanted biomolecules, they are now known to partake in numerous key physiological processes in cancer, such as endocytosis, autophagy, exocytosis, plasma membrane repair, homeostatic maintenance, apoptosis and multidrug resistance. Therefore, in light of this correlation between lysosomes and cancer, lysosomes have been recently considered as a novel target for anticancer therapy. [45, 46] The localization of ZnPc-$(COOH)_8$ and ZPCN were investigated by co-incubating photosensitized cells with lysotracker blue and mitotracker green. As shown in Fig. 4, ZnPc-$(COOH)_8$ and ZPCN localize in the same subcellular region as the lysosome marker, suggesting their affinity to lysosome. These data implied that ZPCN would decompose and release ZnPc-$(COOH)_8$ inside cancer cells.

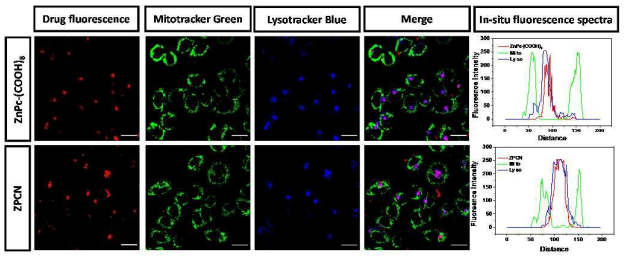

Fig. 4 Localization fluorescence image and in situ fluorescence analysis of ZnPc-$(COOH)_8$ and ZPCN, with different treatment, with lysotracker blue and mitotracker green in cancer cells (Bar = 25 nm).

In vitro anticancer activity

The in vitro anticancer activity of the different drugs against A549 cells were evaluated by MTT assay. As shown in Fig. 5A, cell survival percent of dark incubation cycle for ZPCN was about 85.9%, which is possibly caused by Cu^{2+} mediated anticancer pathway. No obvious dark toxicity was detected in ZnPc-$(COOH)_8$ treated cells. After irradiation (Fig. 5B), cell survival percent of ZnPc-$(COOH)_8$ treated cells was about 55.4%. Almost same cell death percent were detected in Cu^{2+} treated cell before (85.9%) and after irradiation (84.5%). Interestingly, the cell survival decreasing degree of ZPCN (23.7%) was much bigger than the sum effect of ZnPc-$(COOH)_8$ and Cu^{2+}, which indicated that there are that there are additive and synergistic anticancer mechanisms in the anticancer process of ZPCN (synergistic index=1.97) (Table 1).

Defective apoptosis (programmed cell death) represents a major causative factor in the development and progression of cancer. The ability of tumor cells to evade engagement of apoptosis can play a significant role in their resistance to conventional therapeutic regimens. [47] And, failure to undergo apoptosis may result in treatment resistance. [48] Therefore, finding effective ways to induce cancer cells apoptosis could uncover new and effective strategies to tackle the complexity of tumor treatment resistance. The apoptosis-inducing effect of various drugs on A549 cells were detected using Annexin V-FITC/PI apoptosis detection kit. Annexin V-FITC labels the phosphatidylserine sites that translocate to the extracellular membrane upon initiation of apoptosis. PI labels the intracellular DNA in the late apoptotic cells where the plasma membrane has been compromised. Above combination results could differentiate the apoptotic and viable cells by the

Table 1. Dark (ATP depletion process) and light (ATP depletion process + PDT process, a synergistic process) cell toxicity comparison of various drugs. Synergistic index was calculated by dividing the expected growth inhibition rate by the observed growth inhibition rate. An index more than 1 indicates synergistic effect and less than 1 indicates no synergistic effect. [49]

		Dark	Light
Drugs	Cu^{2+}	83.5%	84.5%
	ZnPc-$(COOH)_8$	97.0%	55.4%
	ZPCN	85.9%	23.7%
Expected		---	46.8%
Observed		---	23.7%
Synergistic index		---	1.97

View Article Online
DOI: 10.1039/C8TB00334C

flow cytometry. As shown in Fig. 5C, ZnPc-$(COOH)_8$ and Cu^{2+} showed the apoptosis-inducing characteristics, and the apoptosis ratios were 71.10% and 28.22%, separately. Of note, ZPCN had a prominent apoptosis ratio of 89.41%.

Anticancer mechanism of dark and light cycle

ATP is classified as a nucleoside triphosphate, which indicates that it consists of three components, a nitrogenous base (adenine), the sugar ribose, and the triphosphate. ATP is one of four "monomers" required in the synthesis of RNA. Therefore, DNA replication and DNA transcription also consumes ATP. Besides, ATP is often referred to as the energy supplier for a lot of biological process, such as GSH biosynthesis. Tumor cells need large amount of ATP as energy because of their rapid proliferation and glycolysis. Intracellular ATP concentration sharply decreases could affect ATP needed physiological processes, such as DNA replication and GSH biosynthesis. [50, 51] reports indicated that although tumor cells have selected many mechanisms to escape and resist programmed cell death, they cannot avoid ATP depletion-induced death, which indicated that ATP is very crucial for cell surviving. [23] Cu^{2+} has very strong affinity with phosphate. Therefore, the bond between Cu and COO could be destroyed and replaced by the bond between Cu^{2+} and phosphate in the present of ATP. The Fenton-type reaction, in which copper ion reacts with H_2O_2 (malignant cancerous cells would produce excessive amounts of H_2O_2 and cause significant increase of H_2O_2 level in the tumor microenvironment [34]) to form hydroxyl radical ($^{\cdot}OH$), a reactive oxygen species that can damage ATP and induce ATP depletion inside cells. [35]

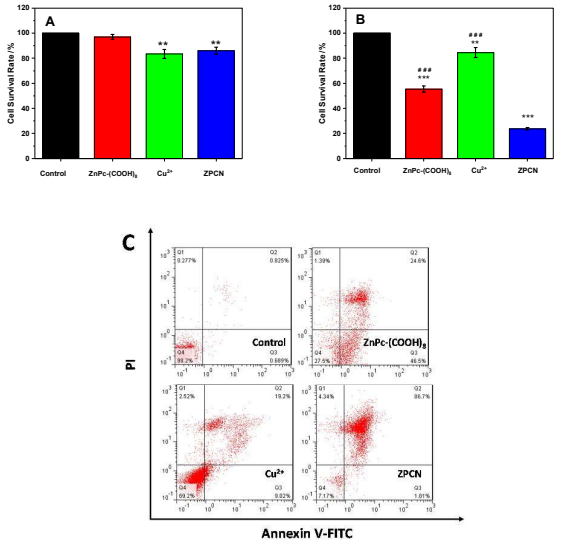

Fig. 5 (A) Dark cell toxicity comparison of various drugs (data are expressed as means ± SD; **P < 0.01 drugs versus control). (B) Light toxicity comparison of various drugs. (Data are expressed as means ± SD; **P < 0.01, ***P < 0.001 drugs versus control; ###P < 0.001 ZnPc-$(COOH)_8$ or Cu^{2+} versus ZPCN). (C) Flow cytometric analysis of A549 cell apoptosis induced by different drugs using Annexin V-FITC/PI staining. In each panel, the lower-left (Q4, Annexin V-FITC$^-$, PI$^-$), lower-right (Q3, Annexin V-FITC$^+$, PI$^-$) and upper-right (Q2, Annexin V-FITC$^+$, PI$^+$) quadrants represent the populations of the viable, early apoptotic and late apoptotic cells, respectively.

To verify this hypothesis, ATP concentration influence by various drugs were studied. In vitro ATP deprivation and hydrolysis of various drugs were carried out using ATP assay kit. Results indicated that the cells incubated with Cu^{2+} and ZPCN could cause obviously ATP concentration decrease (Fig. 6A), and thus lead to energy shortages within the cells under investigation. On the contrary, no obvious changing of ATP decreasing was detected on ZnPc-$(COOH)_8$ treated cell comparing with control cells.

Then, variation of cell cycle arrest induced by various drugs were studied and compared. Almost no cell cycle changing was detected in ZnPc-$(COOH)_8$ treated cell after 48 h dark incubation comparing with the untreated cells. The Cu^{2+} and ZPCN treated cells incubated for 48 h dark incubation displayed arrest in the S phase (Fig. 6C). Fig. 6B shows the statistical data for all of the treatment groups to enable comparison of the proportion of A549 cells arrested in the S phase. DNA replication occurs during this phase. S phase arrest indicated that cell DNA replication inhibition, which is possibly because of the insufficient ATP supplying. Such a notable enhancement in cell cycle arrest of ZPCN shows its potential in combination therapies.

Besides, ATP depletion and $^{\cdot}OH$ generation could also inhibit GSH formation or directly destroy GSH (The GSH depletion is not due to the direct interaction between ZPCN and GSH because spectral results indicated no direct interaction between them, Fig. S3). GSH is an important

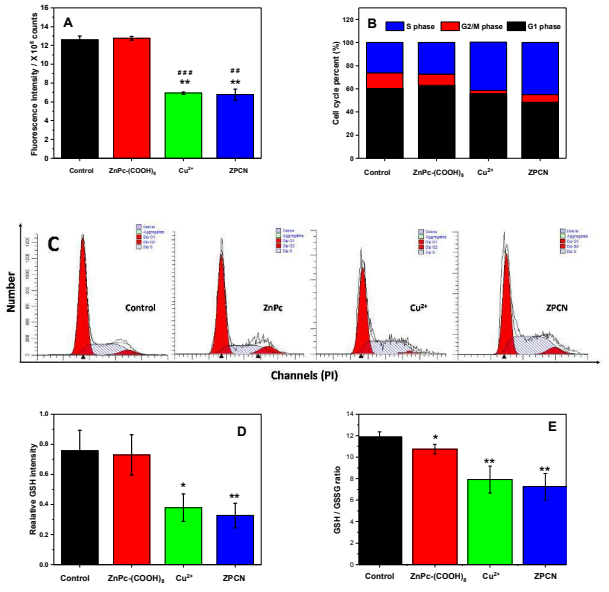

Fig. 6 (A) ATP concentration comparison of various drugs after 48 h dark incubation; (Data are expressed as means ± SD; **P < 0.01, ***P < 0.001 drugs versus control; ##P < 0.01, ###P < 0.001 Cu^{2+} or ZPCN versus ZnPc-$(COOH)_8$) (B) The statistical data for the impact of drugs on the distribution of A549 cell cycle populations after 48 h dark incubation; (C) The impact of drugs on the distribution of A549 cell cycle populations after 48 h dark incubation; (D) GSH level inside cells comparison of various drugs after 48 h dark incubation(*P < 0.05,**P < 0.01, drugs versus control); (E) GSH/GSSG ratio inside cells comparison of various drugs after 48 h dark incubation(*P < 0.05,**P < 0.01, drugs versus control).

View Article Online
DOI: 10.1039/C8TB00334C

antioxidant defence of cells because it could prevent the damage by ROSs. Therefore, GSH in cancer cells could consume ROS and sharply reduce PDT activity. In other words, reducing the GSH concentration inside cells might greatly improve PDT activity. Reports indicated that an increase in GSH or GSH/GSSG is indicative of augmented antioxidant capacity, whereas a decrease is suggestive of diminished antioxidant defences. [52 53]As shown in Fig. 6D and E, Cu^{2+} and ZPCN treated cells all showed GSH and GSH/GSSG decreasing, which indicated that they could diminished the antioxidant defences of cancer cells and helpful for the light cycle PDT process. Based on above results, we could get a conclusion that during the dark cycle of the treatment of ZPCN, ATP in cells was depletion, which induce DNA replication inhibition and antioxidant defence destruction.

We hypothesis that during the light cycle, ROS, including H_2O_2, ·OH, $O_2^{\cdot-}$ and $^1O_2$, was generated inside cancer cells and induced cell death. DCFH-DA is oxidized by total ROS to a fluorescent product, dichlorofluorescein (DCF) [54]. DHE, BES-H_2O_2-AC and SOSG are specific dye for $O_2^{\cdot-}$, H_2O_2 and $^1O_2$. [55-57] As shown in Fig. 7, no obvious $O_2^{\cdot-}$ were detected in all groups, which indicated that it is not the main ROS during this PDT process. No $^1O_2$ generation was detected in Cu^{2+} treated cell. But, Cu^{2+} could increase DCF fluorescence intensity but degrease BES-H_2O_2-AC fluorescence intensity, which indicated that DCF fluorescence intensity increasing was caused by the generated ·OH from the Fenton reaction of Cu (consuming H_2O_2 simultaneously). ZnPc-$(COOH)_8$ generated H_2O_2 during PDT process. Theoretically, H_2O_2 generation by ZPCN should be higher than that of ZnPc-$(COOH)_8$ because of the decreased antioxidant defence of cells. However, the H_2O_2 generation by ZPCN was not higher than that of ZnPc-$(COOH)_8$, which is possibly because the Fenton reaction of released Cu^{2+} consumed the extra H_2O_2. The total ROS generation ability of ZPCN was obviously higher than that of ZnPc-$(COOH)_8$. And such ROS increasing was partly contributed by $^1O_2$ generation capability improving. Furthermore, the decreased antioxidant defence of cells also very helpful for the increasing efficacy. Based on above results, we could get a conclusion that during the light cycle of the treatment of ZPCN, abundant ROS was generated to kill the cancer cells. The dark cycle could not only induce cell death directly, but also provide a weak antioxidant microenvironment for light cycle PDT process.

Mitochondria is a very important ATP and endogenous ROS generate site, so, ATP depletion and extra ROS burst could induce mitochondria dysfunction, which can activate apoptosis pathways capable of inducing cell death. Based on above conception, we proposed that the dark and light cycle could have synergistic effect to induce mitochondria dysfunction and activate apoptosis pathways. The level of mitochondrial rhodamine 123 uptake is directly related to mitochondrial transmembrane potential, an indirect indicator of the mitochondria dysfunction and energetic status of mitochondria.[58] Mitochondrial damage induces quenching or enhancing of rhodamine 123, which is called depolarization or hyperpolarization, and finally induce cell death.

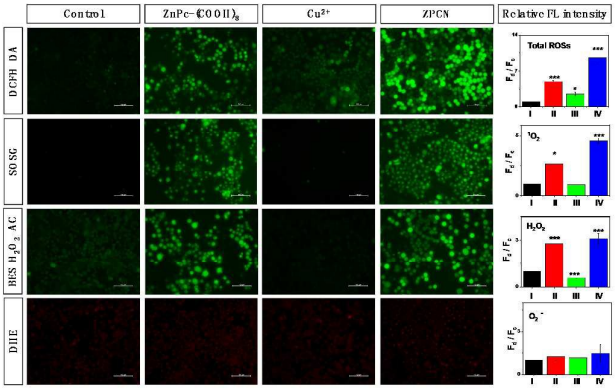

Fig. 7 Fluorescence images and their Normalized average intracellular fluorescence intensity of various ROS generation various drugs and light irradiation (Bar=100 nm, F_d was the fluorescence intensity of drug treated cells, F_c was the fluorescence intensity of control cells, * P<0.05, ** P<0.01, *** P<0.001 drug treated cells vs. control).

As shown in Fig. 8, ATP depletion could induce mitochondrial hyperpolarization. But the effect of ROS burst plus ATP depletion of ZPCN could induce 68.72% cell mitochondria transmembrane potential depolarization, which in much higher that ZnPc-$(COOH)_8$ treated one (49.69%). These results indicated that the anticancer mechanism of ZPCN is a synergistic process rather than being simply aggregated. Mitochondria transmembrane potential depolarization can directly induce cell apoptosis. Therefore, the synergistic of above cycles could cause mitochondrial dysfunction and induce effective cell apoptosis under hypoxic condition.

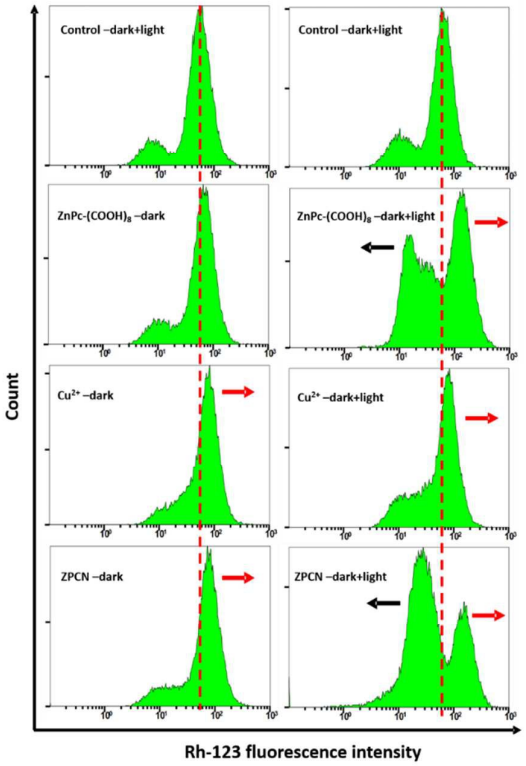

Fig. 8 Rhodamine 123 fluorencense changing of varies drug.

View Article Online
DOI: 10.1039/C8TB00334C

In vivo biocompatibility and anticancer activity

The in vivo biocompatibility of ZnPc-$(COOH)_8$ and ZPCN was very important for their safety using guarantee. Healthy female Kunming mice were intravenously injected with ZnPc-$(COOH)_8$ or ZPCN. The group intravenously injected with saline was set as the control group. The body weights of the mice were recorded every day and the results indicated that no obvious body-weight losing during 20 days treating (Fig. 9A). Besides, the tissue sections of heart, liver, spleen, lung, kidney and brain stained by H&E showed no apparent pathological changes (Fig. 9B). These preliminary data indicate the high biocompatibility of ZnPc-$(COOH)_8$ and ZPCN.

The in vivo anticancer efficiency assessed on A549 tumor xenograft in nude mice. The tumor bearing mice were divided into 3 groups: control, ZnPc-$(COOH)_8$ and ZPCN treated groups. After the intravenous administration of drugs for 6 h, 665 nm light was directly irradiated on the tumor position. As shown in Fig. 9C, no obvious body-weight losing was detected after treating by ZnPc-$(COOH)_8$ or ZPCN comparing with control group during 20 days treatment. On the contrary, the tumorgrowth was significantly suppressed in the ZnPc-$(COOH)_8$ and ZPCN treated group compared to the control groups (Fig. 9D). In the H&E stained tumor section, only a small portion of purple blue (nuclei stained by hematoxylin) area in the ZPCN treated mice, which was obviously smaller than ZnPc-$(COOH)_8$ treated one and the control group.

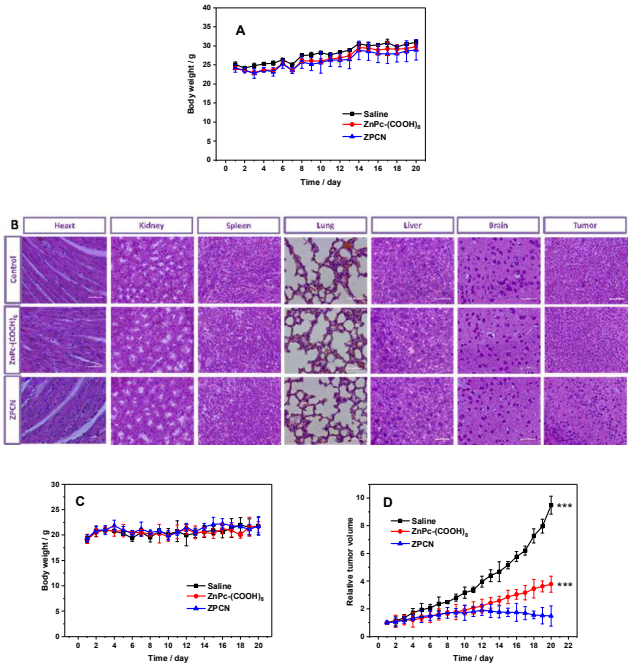

Fig. 9 (A) Kunming mice body weight change as a function of feeding time after ZnPc-$(COOH)_8$, ZPCN or saline treatment; (B) H&E stained histological sections of heart, liver, spleen, lung, kidney and brain from the Kunming mice and H&E stained histological sections of tumor from BALB/c nude mice the after 20 days treating (Bar =100 μm); (C) BALB/c nude mice body weight change as a function of drugs and light treating time after drugs treatment; (D) tumor-volume change as a function of drugs and light treating time after treating with ZnPc-$(COOH)_8$, ZPCN or saline and 665 nm irradiation (*** $P<0.001$ ZPCN treated cells vs. control or ZnPc-$(COOH)_8$ treated cells).

Conclusions

Solid tumors hypoxic microenvironment is believed to be one of the major causes for the failure of PDT. Therefore, finding new PDT system with high activity under hypoxia condition has attracted great attention during past years. Classic solutions were based on directly increasing in situ O_2 concentration combining PS with a hypoxia-activated prodrug. In this manuscript, a new strategy was exploited based on ATP depletion. ATP generation route for hypoxia tumor cells was an ineffective glycolysis processes, but ATP is very important for rapid and uncontrolled growing and dividing. Therefore, finding effective ways to deplete ATP could make cancer cell weak and sensitive. Based on this concept, we prepared a nanoscale metal-organic framework nanoparticle ZPCN, which could deplete ATP after entrapped by cancer cells and induce satisfied PDT activity. Our research demonstrated the potential applicability of the new strategy to overcome hypoxic tumor treatment by PDT.

Conflicts of interest

There are no conflicts to declare.

Acknowledgements

This research was financially supported by the National Natural Science Foundation of China (NO. 21571105 and 21671105), the project BK20161554 supported by NSF of Jiangsu Province of China. The Priority Academic Program Development of Jiangsu Higher Education Institutions (PAPD), the Foundation of Jiangsu Collaborative Innovation Centre of Biomedical Functional Materials (161090H001).

Notes and references

1. C. Zhang, K. Zhao, W. Bu, D. Ni, Y. Liu, J. Feng and J. Shi, *Angew. Chem. Int. Edit.*, 2015, **54**, 1770-1774.
2. M. Lismont, L. Dreesen and S. Wuttke, *Adv. Fun. Mater.*, 2017, **27**,1606314.
3. I. Roy, T. Y. Ohulchanskyy, H. E. Pudavar, E. J. Bergey, A. R. Oseroff, J. Morgan, T. J. Dougherty and P. N. Prasad, *J. Am. Chem. Soc.*, 2003, **125**, 7860-7865.
4. H. Chen, J. Tian, W. He and Z. Guo, *J. Am. Chem. Soc.*, 2015, **137**, 1539-1547.
5. W. L. Lu, Y. Q. Lan, K. J. Xiao, Q. M. Xu, L. L. Qu, Q. Y. Chen, T. Huang, J. Gao and Y. Zhao, *J. Mater. Chem. B.*, 2017, **5**, 1275-1283.
6. E. Ju, K. Dong, Z. Liu, F. Pu, J. Ren and X. Qu, *Adv. Fun. Mater., 2015, 25, 1574-1580.*
7. M. Wartenberg, F. C. Ling, M. Muschen, F. Klein, H. Acker, M. Gassmann, K. Petrat, V. Putz, J. Hescheler and H. Sauer, *FASEB J.*, 2003, **17**, 503.
8. H. Tian, Z. Luo, L. Liu, M. Zheng, Z. Chen, A. Ma, R. Liang, Z.

View Article Online
DOI: 10.1039/C8TB00334C

Han, C. Lu and L. Cai, *Adv. Fun. Mater.*, 2017, **27**, 1703197.
9. G. Song, C. Liang, X. Yi, Q. Zhao, L. Cheng, K. Yang and Z. Liu, *Adv. Mater.,* 2016, **28**, 2716-2723.
10. J. Zhou, T. Schmid, R. Frank and B. Brune, *J. Biol. Chem.*, 2004, **279**, 13506-13513.
11. Z. Wang, S. Li, M. Zhang, Y. Ma, Y. Liu, W. Gao, J. Zhang and Y. Gu, *Adv. Sci.*, 2017, **4**, 1600327.
12. Y. Liu, Y. Liu, W. Bu, Q. Xiao, Y. Sun, K. Zhao, W. Fan, J. Liu and J. Shi, *Biomaterials*, 2015, **49**, 1-8.
13. Y. Zhang, F. Wang, C. Liu, Z. Wang, L. Kang, Y. Huang, K. Dong, J. Ren and X. Qu, *Acs Nano*, 2018, 651-661.
14. A. Srivatsan, J. R. Missert, S. K. Upadhyay and R. K. Pandey, *J. Porphyr. Phthalocya.*, 2015, **19**, 109-134.
15. C. Qian, J. Yu, Y. Chen, Q. Hu, X. Xiao, W. Sun, C. Wang, P. Feng, Q. D. Shen and Z. Gu, *Adv. Mater.*, 2016, **28**, 3313-3320.
16. D. Zhang, M. Wu, Y. Zeng, N. Liao, Z. Cai, G. Liu, X. Liu and J. Liu, *J. Mater. Chem. B*, 2016, **4**, 589-599.
17. Y. Cheng, H. Cheng, C. Jiang, X. Qiu, K. Wang, W. Huan, A. Yuan, J. Wu and Y. Hu, *Nat. Commun.*, 2015, **6**.8785.
18. W. Fan, W. Bu, B. Shen, Q. He, Z. Cui, Y. Liu, X. Zheng, K. Zhao and J. Shi, *Adv. Mater.*, 2015, **27**, 4155-4161.
19. M. Gao, C. Liang, X. Song, Q. Chen, Q. Jin, C. Wang and Z. Liu, *Adv. Mater.*, 2017, **29**, 1701429.
20. L. Feng, L. Cheng, Z. Dong, D. Tao, T. E. Barnhart, W. Cai, M. Chen and Z. Liu, *Acs Nano.*, 2017, **11**, 927-937.
21. Y. Liu, Y. Liu, W. Bu, C. Cheng, C. Zuo, Q. Xiao, Y. Sun, D. Ni, C. Zhang, J. Liu and J. Shi, *Angew. Chem. Int. Edit.*, 2015, **54**, 8105-8109.
22. S. Tuncel, A. Trivella, D. Atilla, K. Bennis, H. Savoie, F. Albrieux, L. Delort, H. Billard, V. Dubois, V. Ahsen, F. Caldefie-Chezet, C. Richard, R. W. Boyle, S. Ducki and F. Dumoulin, *Mol. Pharmaceutics*, 2013, **10**, 3706-3716.
23. J. Pouyssegur, F. Dayan and N. M. Mazure, *Nature*, 2006, **441**, 437-443.
24. A. M. Poveda, M. Le Clech and P. Pasero, *Transcription*, 2010, **1**, 99-102.
25. H. Fan, G. Yan, Z. Zhao, X. Hu, W. Zhang, H. Liu, X. Fu, T. Fu, X.-B. Zhang and W. Tan, *Angew. Chem. Int. Edit.*, 2016, **55**, 5477-5482.
26. J. Marx, *Science*, 1994, **263**, 319-321.
27. Y. Ma, X. Li, A. Li, P. Yang, C. Zhang and B. Tang, *Angew. Chem. Int. Edit.*, 2017, **56**, 13752-13756.
28. Y. M. Zhang and J. F. Lovell, *Wires. Nanomed. Nanobi*, 2017, **9**: e1420.
29. L. Wang, Q. Song, Q. Liu, D. He and J. Ouyang, *Adv. Fun. Mater.*, 2015, **25**, 7017-7027.
30. C. Walling and S. Kato, *J. Am. Chem. Soc.*, 1971, **93**, 4275-4281.
31. Y. Ohta, N. Shiraishi, T. Nishikawa and M. Nishikimi, *BBA-Gen. Subjects.*, 2000, **1474**, 378-382.
32. B. Halliwell, *The Lancet*, 1994, **344**, 721-724.
33. S. Karthik, A. Jana, M. Selvakumar, Y. Venkatesh, A. Paul, S. S. Shah and N. D. P. Singh, *J. Mater. Chem. B.*, 2017, **5**, 1734-1741.
34. G. Song, Y. Chen, C. Liang, X. Yi, J. Liu, X. Sun, S. Shen, K. Yang and Z. Liu, *Adv. Mater.,* 2016, **28**, 7143-71487.
35. Y. Ohta, N. Shiraishi, T. Nishikawa and M. Nishikimi, *Biochim. Biophys. Acta*, 2000, **1474**, 378-382.
36. E. Ju, K. Dong, Z. Chen, Z. Liu, C. Liu, Y. Huang, Z. Wang, F. Pu, J. Ren and X. Qu, *Angew. Chem. Int. Edit.,* 2016, **55**, 11639–11643.
37. Q. Zhan, X. Shi, X. Yan, Q. Liu, J. Zhou, L. Zhou and S. Wei, *J. Mater. Chem*. B., 2017, **5**, 6752-6761
38. L. Zhou, E. Chen, W. Jin, Y. Wang, J. Zhou and S. Wei, *Dalton T.,* 2016, **45**, 15170-15179.
39. B. Thienpont, J. Steinbacher, H. Zhao, F. D'Anna, A. Kuchnio, A. Ploumakis, B. Ghesquiere, L. Van Dyck, B. Boeckx, L. Schoonjans, E. Hermans, F. Amant, V. N. Kristensen, K. P. Koh, M. Mazzone, M. L. Coleman, T. Carell, P. Carmeliet and D. Lambrechts, *Nature*, 2016, **537**, 63-68.
40. J. Yang, J. Zhao, Q. Cao, L. Hao, D. Zhou, Z. Gan, L. Ji and Z. Mao, *ACS appl. Mater. Inter.,* 2017, **9**, 13900-13912.
41. S. Dong, H. Tian, L. Huang, J. Zhang, D. Yan, Y. Geng and F. Wang, *Adv. Mater.*, 2011, **23**, 2850–2854.
42. Z. Zeng, J. Zhou, Y. Zhang, R. Qiao, S. Xia, J. Chen, X. Wang and B. Zhang, *J. Phys. Chem. B.*, 2007, **111**, 2688-2696.
43. C. L. Yu, S. J. Xu, S. Chen, M. H. Zhang and T. Shen, *J. Photoch. Photobio.B*., 2002, **68**, 73-78.
44. T. Jiang, R. Mo, A. Bellotti, J. Zhou and Z. Gu, *Adv. Funct. Mater.*, 2014, **24**, 2295-2304.
45. B. Zhitomirsky and Y. G. Assaraf, *Drug Resist. Update.*, 2016, **24**, 23-33.
46. N. Seebacher, D. J. R. Lane, D. R. Richardson and P. J. Jansson, *Free Radical Bio. Med.*, 2016, **96**, 432-445.
47. S. Kasibhatla and B. Tseng, *Mol. Cancer Ther.*, 2003, **2**, 573-580.
48. S. Fulda and K. M. Debatin, *Oncogene*, 2006, **25**, 4798-4811.
49. D. H. Shin, H.-Y. Min, A. K. El-Naggar, S. M. Lippman, B. Glisson and H.-Y. Lee, *Mol. Cancer Ther.*, 2011, **10**, 2437-2448.
50. E. L. Hansen, E. B. Sozer, S. Romeo, S. K. Frandsen, P. T. Vernier and J. Gehl, *PloS one*, 2015, **10**, e0122973.
51. M. A. Moro, A. Almeida, J. P. Bolaños and I. Lizasoain, *Free Radical Bio. Med.*, 2005, **39**, 1291-1304.
52. Y. Zhou, D. E. Harrison, K. Love-Myers, Y. Chen, A. Grider, K. Wickwire, J. R. Burgess, M. A. Stochelski and R. Pazdro, *Free Radical Bio. Med.*, 2014, **71**, 157-164.
53. J. Yang, Y. Duan, X. Zhang, Y. Wang and A. Yu, *J. Mater. Chem. B.*, 2016, **4**, 3868-3873.
54. Y. Zhao, C. Ye, W. Liu, R. Chen and X. Jiang, *Angew. Chem. Int. Edit.*, 2014, **53**, 8127-8131.
55. Z. Zhang, S. S. Leonard, C. S. Huang, V. Vallyathan, V. Castranova and X. L. Shi, *Free Radical Bio. Med.*, 2003, **34**, 1333-1342.
56. H. Kanzaki, F. Shinohara, M. Kajiya, S. Fukaya, Y. Miyamoto and Y. Nakamura, *Free Radical Bio. Med.*, 2014, **77**, 239-248.
57. Z. Zhu, Z. Tang, J. A. Phillips, R. Yang, H. Wang and W. Tan, *J. Am. Chem. Soc.*, 2008, **130**, 10856-10857.
58. R. J. Mark, J. N. Keller, I. Kruman and M. P. Mattson, *Brain Res.*, 1997, **756**, 205-214.